THE JOURNAL OF PHYSICAL CHEMISTRY B

Article

pubs.acs.org/JPCB

Importance of Polar Solvation and Configurational Entropy for Design of Antiretroviral Drugs Targeting HIV-1 Protease

Parimal Kar,[†] Reinhard Lipowsky, and Volker Knecht*[,‡]

Department of Theory and Bio-Systems, Max Planck Institute of Colloids and Interfaces, Am Mühlenberg 1, 14476 Potsdam, Germany

Supporting Information

ABSTRACT: Both KNI-10033 and KNI-10075 are high affinity preclinical HIV-1 protease (PR) inhibitors with affinities in the picomolar range. In this work, the molecular mechanics Poisson−Boltzmann surface area (MM-PBSA) method has been used to investigate the potency of these two HIV-1 PR inhibitors against the wild-type and mutated proteases assuming that potency correlates with the affinity of the drugs for the target protein. The decomposition of the binding free energy reveals the origin of binding affinities or mutation-induced affinity changes. Our calculations indicate that the mutation I50V causes drug resistance against both inhibitors. On the other hand, we predict that the mutant I84V causes drug resistance against KNI-10075 while KNI-10033 is more potent against the I84V mutant compared to wild-type protease. Drug resistance arises mainly from unfavorable shifts in van der Waals interactions and configurational entropy. The latter indicates that neglecting changes in configurational entropy in the computation of relative binding affinities as often done is not appropriate in general. For the bound complex PR_{I50V}−KNI-10075, an increased polar solvation free energy also contributes to the drug resistance. The importance of polar solvation free energies is revealed when interactions governing the binding of KNI-10033 or KNI-10075 to the wild-type protease are compared to the inhibitors darunavir or GRL-06579A. Although the contributions from intermolecular electrostatic and van der Waals interactions as well as the nonpolar component of the solvation free energy are more favorable for PR−KNI-10033 or PR−KNI-10075 compared to PR−DRV or PR−GRL-06579A, both KNI-10033 and KNI-10075 show a similar affinity as darunavir and a lower binding affinity relative to GRL-06579A. This is because of the polar solvation free energy which is less unfavorable for darunavir or GRL-06579A relative to KNI-10033 or KNI-10075. The importance of the polar solvation as revealed here highlights that structural inspection alone is not sufficient for identifying the key contributions to binding affinities and affinity changes for the design of drugs but that solvation effects must be taken into account. A detailed understanding of the molecular forces governing binding and drug resistance might assist in the design of new inhibitors against HIV-1 PR variants that are resistant against current drugs.

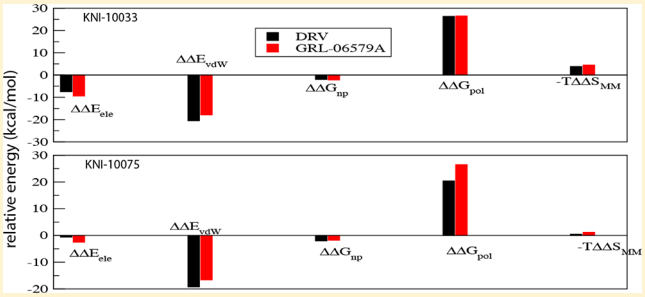

1. INTRODUCTION

Acquired immune deficiency syndrome or AIDS is caused by the human immunodeficiency virus (HIV). The World Health Organization (WHO) has classified AIDS as a pandemic. HIV type 1 protease (HIV-1 PR) is responsible for the cleavage of the viral *gag* and *pol* polyproteins into mature and functional proteins. Since inhibition of the HIV-1 PR activity prevents the maturation of these viral proteins and, thus, the replication of the virus, HIV-1 PR has been an important target for anti-AIDS drug therapy.

The HIV-1 PR is a homodimeric aspartic protease composed of residues 1−99 and 1′−99′ (see Figure 1). Each monomer contains an α-helix and two antiparallel β-sheets. The active site is evolutionary conserved and composed of the conserved catalytic triad, Asp25(25′)−Thr26(26′)−Gly27(27′). The enzyme active site is gated by two extended β hairpin loops (residues 46−56), known as the flap regions, which presumably open and close to allow entry and binding of substrates.[1]

Up to now, no cure exists to eliminate AIDS. However, with the introduction of highly active antiretroviral drugs, the treatment of HIV/AIDS patients has been improved, effectively decreasing the mortality rate of HIV/AIDS patients.[2] The treatment consists of a combination of at least three selected drugs that inhibit (i) the HIV replication cycle at the point of entry (chemokine antagonists, fusion inhibitors), (ii) its reverse transcription (nucleoside reverse transcriptase inhibitor or nonnucleoside reverse transcriptase inhibitor), and (iii) its integration (integrase inhibitor) or viral production (protease inhibitor). Developing vaccines to fight the AIDS infection is challenging.[3] So far, nine protease inhibitors have been approved by the Food and Drug Administration (FDA) for HIV therapy. These drugs are saquinavir (SQV), ritonavir

Received: August 28, 2012
Revised: April 9, 2013
Published: April 24, 2013

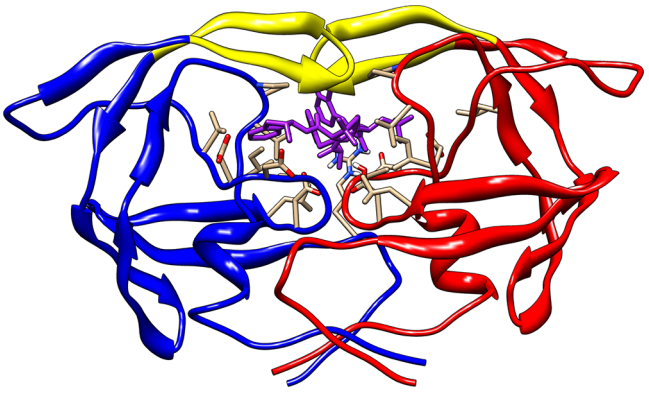

Figure 1. Wild-type HIV-1 protease dimer with bound drug KNI-10033 (magenta). The protein is shown in ribbon representation where the monomers are distinguished by different colors (blue and red). Residues at the binding site (gray and red), as well as the inhibitor (magenta), are depicted as sticks. The flap regions are shown in yellow color.

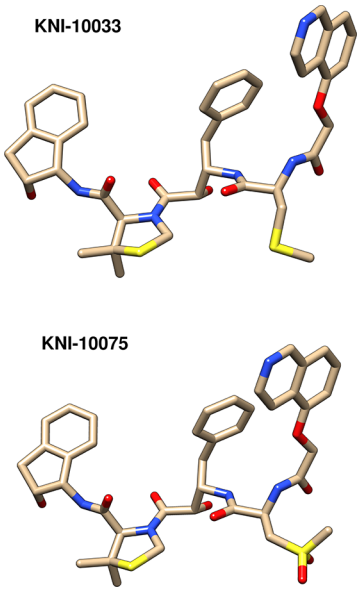

Figure 2. Chemical structure of KNI-10033 (top) and KNI-10075 (bottom) in stick representation. Colors distinguish between carbon (gray), oxygen (red), nitrogen (blue), and sulfur (yellow).

(RTV), indinavir (IDV), nelfinavir (NFV), amprenavir (APV), lopinavir (LPV), atazanavir (AZV), tipranavir (TPV), and darunavir (DRV). However, the effectiveness of these inhibitors is limited by the occurrence of drug resistant mutations in the target enzyme caused by the high replication rate of HIV-1 and the lack of a proof-reading mechanism in its reverse transcriptase (RT).[4] To date, over 50 different drug resistance mutations at almost 30 different codon positions of HIV-1 PR have been characterized,[5] mainly arising due to the gene's highly polymorphic nature. Even in the absence of antiretroviral drugs, HIV is genetically diverse, especially in the protease gene that showed variations in up to 50 different residues.[6]

In the present study, we have addressed the binding of the two preclinical protease inhibitors (PIs) KNI-10033 and KNI-10075 with the wild-type protease and predict the binding free energies for a variety of mutants. The chemical structures of KNI-10033 and KNI-10075 are shown in Figure 2. Both inhibitors are identical except for a single substitution: the $-S-CH_3$ group in KNI-10033 is replaced by a $-SO_2CH_3$ group in KNI-10075.[7]

The HIV-1 resistance against protease inhibitors arises mainly due to the occurrence of mutations in the protease that significantly impair the protease's interaction with drugs but impair neither the substrate binding nor the product unbinding process nor the interaction with the transition state of the enzymatic reaction. Mutations could occur at residues directly interacting with the inhibitors or far away from the inhibitor binding site.[8] These drug-resistant protease variants lose their high binding affinity to the inhibitors while maintaining sufficient enzyme activity for the virus to propagate. Conservative mutations of hydrophobic residues are common in protease inhibitor resistance, including I50V and I84V, which have been experimentally found to be resistant against a variety of drugs. Here, we investigate the resistance of these two mutants against the new protease inhibitors KNI-10033 and KNI-10075, using computational methods.

To understand the mechanism underlying the binding of KNI-10033 and KNI-10075 to wild-type protease and its mutant variants from an energetic point of view, we have used molecular dynamics simulations and free energy calculations to study the contributions to the binding affinities for the respective complexes. The most rigorous and accurate methods to calculate binding free energies such as free energy perturbation (FEP),[9] thermodynamic integration (TI),[10] metadynamics,[11] and umbrella sampling[12] are computationally very expensive. One limitation of pathway methods including metadynamics is the necessity to choose one or a few appropriate reaction coordinates which often is nontrivial. In addition, the time scales needed for convergence depend on the suitability of the reaction coordinates. In contrast, the MM-PBSA method[13−15] is faster by several orders of magnitude than FEP or TI. The MM-PBSA scheme is applied here. Theoretical considerations within the framework of MM/PBSA are particularly useful for this type of investigation because they allow insight into structural details otherwise inaccessible to experimental techniques. Moreover, MM/PBSA is particularly appropriate for this case because HIV-1 PR is located in the cytosol; hence, the binding will take place in aqueous solution for which the employed models have been optimized over many years.

In MM-PBSA methods, the binding free energy is estimated from molecular mechanical energies and solvation free energies for an ensemble of molecular configurations as obtained from molecular dynamics simulations in explicit water. The MM-PB(GB)SA methods have successfully been used to estimate the binding free energies of protein−ligand[16,17] and protein−RNA[18,19] complexes. These methods have also been used to study the binding of different inhibitors to protease[20,21] and reverse transcriptase (RT).[22] Recently, Worch et al.[23] have modeled the interaction propensity of transmembrane domain (TMD) pairs and computed free energies for TMD dimer formation using the MM-PBSA approach. Compared to our study, the PBSA term was replaced with the multiple continua approach established to mimic biomembrane environments, with the aqueous domain modeled by water, the polar headgroup region by ethanol, and the hydrophobic core by cyclohexane.[24] In our study, the contribution from the change in entropy of the binding partners was obtained from a normal-mode analysis[25,26] of the complex and the individual binding partners. The results of our calculations agree well with

dx.doi.org/10.1021/jp3085292 | J. Phys. Chem. B 2013, 117, 5793−5805

available experimental data and give insights into the origins of mutation-induced affinity changes and, thus, into the molecular mechanisms underlying drug resistance. Our findings also highlight the importance of the polar solvation free energy and the configurational entropy for the design of antiretroviral drugs targeting HIV-1 PR.

2. MATERIALS AND COMPUTATIONAL METHODS

The affinities of HIV-1 PR−inhibitor complexes were evaluated by simulating the complexes in explicit water and calculating the free energies of the resulting configurations using an implicit solvent model.

2.1. Structure Generation with MD Simulations in Explicit Water. The initial coordinates for our simulations were obtained from the X-ray crystallographic structures of the HIV-1 protease (PR) complexed with the inhibitors KNI-10033 and KNI-10075. Recently, Lafont and co-workers[7] have determined X-ray crystallographic structures of the wild-type HIV-1 PR complexed with the two inhibitors at 1.45 and 1.90 Å resolution, respectively, to analyze the molecular basis for their antiviral potency. The corresponding atomic coordinates with the Protein Data Bank accession code 2PK6 for HIV-1 PR−KNI-10033 and 2PK5 for PR−KNI-10075 were used for our current study. All crystal water molecules in the crystal structure of the protease−inhibitor complexes were kept in the starting model. The I50V and I84V mutations were performed manually. Some residues in the PDB structure 2PK6 contain atoms, for which alternative coordinates (A and B) have been assigned. In our study, the A variant was always chosen manually.

The proteins were described using the Amber ff03 force field,[27] the ligand was described by the generalized Amber force field (GAFF),[28] and AM1-BCC[29] atomic charges were calculated with the *antechamber*[30] module of Amber.[31] Our previous studies[32−36] show that this charge scheme is suitable for this kind of study.

The configurations were generated via simulations of the complexes in explicit water. Each complex was solvated in TIP3P water[37] using a truncated octahedron periodic box, extending at least 10 Å from the complex. Nearly 9700 water molecules were added to solvate the complex, and the resulting box size was nearly 89 Å × 89 Å × 89 Å. An appropriate number of chloride ions was added to keep the total system charge neutral. All bond lengths involving hydrogen atoms were constrained using the SHAKE algorithm,[38] allowing the usage of a 2 fs time-step. The temperature was kept fixed at 300 K using a Langevin thermostat with a collision frequency of 2 ps^{-1}. The electrostatic interactions were treated using the particle-mesh Ewald (PME) scheme[39] with a fourth-order B-spline interpolation and a tolerance of 10^{-5}. The nonbonded cutoff was 8 Å, and the nonbonded pair list was updated every 50 fs.

Our simulations were carried out according to the following protocol: (i) Each complex was first optimized by 500 steps of steepest descent followed by another 500 steps of conjugate gradient minimization, keeping all atoms of the complex restrained to their initial position with a weak harmonic potential. (ii) After the minimization, each system was simulated for 50 ps at constant volume with a 2 $kcal{\cdot}mol^{-1}{\cdot}Å^{-2}$ restraint on the complex, in order to equilibrate the solvent at 300 K without undesirable drifts of the structure. (iii) Subsequently, a 50 ps MD simulation with a 2 $kcal{\cdot}mol^{-1}{\cdot}Å^{-2}$ restraint on each complex at a pressure of 1 atm was conducted to relax the density using Berendsen's barostat. (iv) Then, each complex was equilibrated for 1 ns without restraint. After the equilibration phase, a 10 ns simulation at constant pressure was carried out and the coordinates were stored every 10 ps, resulting in 1000 configurations for each simulation. The same protocol has been used in our previous studies.[33−35]

2.2. MM-PBSA Calculations. In the MM-PBSA method, the binding free energy of the protein−ligand complex, ΔG_{bind}, is determined from

$$\Delta G_{bind} = G_{complex} - (G_{receptor} + G_{ligand}) \quad (1)$$

where $G_{complex}$, $G_{receptor}$, and G_{ligand} denote the absolute free energy of the complex, receptor/protein, and ligand, respectively. The free energy G for each species is calculated from

$$G = H - TS = E_{MM} + G_{solv} - TS \quad (2)$$

Here, E_{MM} is the molecular mechanical energy in the gas phase, G_{solv} the solvation free energy, and $-TS$ the contribution from the conformational entropy. The term E_{MM} consists of the internal (bond, angle, dihedral) (E_{int}), electrostatic (E_{elec}), and van der Waals energies (E_{vdW}), according to

$$E_{MM} = E_{int} + E_{vdW} + E_{elec} \quad (3)$$

To incorporate all possible nonbonded interactions, the term E_{MM} was estimated for each snapshot with no cut-offs. The solvation energy, G_{solv}, is composed of an electrostatic (polar) contribution, G_{pol}, and a nonpolar contribution, G_{np}, according to

$$G_{solv} = G_{pol} + G_{np} \quad (4)$$

Here, G_{pol} is estimated from a solution of the linear Poisson−Boltzmann (PB) equation, and the nonpolar solvation term (G_{np}) is evaluated from[40]

$$G_{np} = \gamma A + b \quad (5)$$

where γ is the surface tension proportionality and was set to 0.00542 $kcal{\cdot}mol^{-1}{\cdot}Å^{-2}$ and b is the offset value, which was 0 here. The symbol A denotes the solvent accessible surface area (SASA) which was estimated with a fast linear combination of pairwise overlap (LCPO) algorithm[41] using a probe radius of 1.4 Å.

The averages in eq 2 are calculated from an ensemble of molecular configurations taken from a molecular dynamics simulation to capture the effects of motion. To reduce time consumption and to obtain stable energies, only the complex was simulated. Therefore, E_{int} cancels out in the calculation of G_{bind}.

To account for the molecular structure of water, explicit crystal water molecules were included in our free energy calculations and explicit water molecules were considered as a part of the receptor. Thus, the binding free energy could be obtained from the following equation, which is a standard MM-PBSA approach for including selected solvent molecules:

$$\Delta G_{bind} = G_{complex+WAT} - [G_{receptor+WAT} + G_{ligand}] \quad (6)$$

The electrostatic contribution to the solvation free energy (ΔG_{pol}) was estimated from the Poisson−Boltzmann (PB) approach using the adaptive Poisson−Boltzmann solver (APBS).[42] In order to solve the PB equation, the grid spacing was set to 0.5 Å in all dimensions and the relative dielectric constants in the protein and in the water were chosen to be 1

dx.doi.org/10.1021/jp3085292 | J. Phys. Chem. B 2013, 117, 5793−5805

and 80, respectively. The ionic strength was set to 0.15 M. The ratio between the longest dimension of the rectangular finite-difference grid and that of the solute was chosen to be 4.0. The linear PB equation was solved with a maximum of 1000 iterations.

The MM/PBSA predictions are very sensitive to the solute dielectric constant. In MM-GBSA or MM-PBSA, the dielectric constant of unity (1.0) is normally used for solute. On the other hand, for a highly charged binding interface, a higher solute dielectric constant (ε = 4.0) is recommended by Hou et al.[43] For a moderately charged binding interface, a moderate solute dielectric constant (ε = 2.0) is preferred, while a low solute dielectric constant (ε = 1.0) is suggested for a hydrophobic interface.[43] In previous MM/PBSA calculations of HIV-1 protease, values of 1,[33,34,44] 2,[45,46] and 4[47] have been used for the internal dielectric constant. Recently, Stoica et al.[48] found that the binding enthalpies corresponding to an internal dielectric constant of 1, combined with the entropic contribution, produce overall energies closest to experimental affinities. A similar result was obtained by us in our previous studies of HIV-1 protease.[33,34] In the absence of entropy terms, computed binding enthalpies need to be scaled down to be brought within the range of experimental data, for instance, via a high internal dielectric constant,[49] because of the enthalpy/entropy compensation.[50] Our results on the internal dielectric constant can therefore be interpreted as a consequence of explicitly incorporating conformational sampling, including entropic effects, in the evaluation of binding energies.

The entropy from the vibrational degrees of freedom was calculated by normal-mode analysis (NMA) using the Amber *mmpbsa_py_nabnmode* program. To this aim, 200 configurations were selected; each configuration was energy minimized with a generalized-Born solvent model (nmode_igb = 1) with a maximum of 50 000 steps and a target root-mean-square (rms) gradient of 10^{-4} kcal·mol^{-1}·Å^{-1}.

In order to understand the inhibitor−residue interaction in more detail, the interaction energy was further decomposed into the contributions from each residue of the protease by using the theory of free energy decomposition.[51] To this aim, the less accurate but more efficient MM-GBSA scheme was used. The inhibitor−residue interaction is approximated by

$$\Delta G_{\text{inhibitor}-\text{residue}} = \Delta E_{\text{vdW}} + \Delta E_{\text{elec}} + \Delta G_{\text{GB}} + \Delta G_{\text{np}} \quad (7)$$

where ΔE_{vdW} and ΔE_{elec} are the contributions from the van der Waals and electrostatic interactions between the inhibitor and each residue in the gas phase. The polar solvation free energy, ΔG_{GB}, was estimated by using the generalized Born model. On the other hand, the nonpolar component of the solvation free energy, ΔG_{np}, was computed from the solvent accessible solvent area (A) using eq 5 with γ = 0.0072 kcal·mol^{-1}·Å^{-2} and b = 0.92 kcal/mol.

Experimental binding free energies for the wild-type were calculated from inhibition constants K_i reported by Lafont et al.[7] using

$$\Delta G_{\text{exp}} = -RT \ln K_i \quad (8)$$

with K_i given in M^{-1}. However, inhibition constants for the mutant variants were not available.

3. RESULTS AND DISCUSSION

In order to elucidate the mechanisms underlying the binding of these two different inhibitors to the wild-type protease and its variants, an energetic analysis using a combined MD/MM-PBSA approach was conducted. Molecular configurations obtained from MD simulations of the complexes in explicit water were used for the calculation of binding free energies. 1000 configurations were used in the MM-PBSA calculation.

3.1. Protonation State from pK_a Calculations. The Asp dyad, Asp25 and Asp25′, constitutes the active site base; it is planar and interacts directly with substrates and inhibitors. Of particular importance is the protonation state of the Asp dyad because of its direct contact with the substrate and the inhibitors. The Asp residues in the dyad can be either both unprotonated or both protonated, or only Asp25 or only Asp25′ could be protonated. Since the X-ray crystallographic structures do not contain hydrogen atoms, information about the protonation state cannot be directly obtained from the X-ray data. In order to pinpoint the likely experimental protonation state, we calculated pK_a values for the Asp25 dyad using PROPKA;[52] the results are shown in Table 1. The predicted pK_a values are 10.47−10.50 for Asp25 and 4.24−4.28 for Asp25′. Hence, at pH 5.6, where the binding affinities and the structures of the PR−inhibitor complexes were studied experimentally, Asp25 is most likely protonated and Asp25′ is in the deprotonated state (COO^-). Thus, this asymmetric protonation state is considered in our simulations of the dimer−ligand complexes. Although the unbound form corresponds to a symmetric homodimer, it could be characterized by alternating asymmetric protonation states of the Asp dyad.[53] Our results are consistent with past calculations[33,34,45,48,54] and experimental work.[53]

Table 1. pK_a Values for Asp25/Asp25′ in the Presence of the Inhibitors Obtained from PROPKA[52]

inhibitor	Asp25	Asp25′
PR/KNI-10033	10.50	4.24
PR/KNI-10075	10.47	4.28

3.2. Structural Stability and Flexibility of Wild-Type and Mutant PR Complexes. The production simulations of 10 ns carried out for these systems were stable in terms of the total and potential energies of these systems (data not shown) and the root-mean-square deviation (RMSD) from the X-ray structures (see Figure 3). The average root-mean-squared deviations for the backbone atoms from the corresponding X-ray crystal structure in the simulations are given in Table 2. Their average RMSD values are 1.12, 1.30, and 1.16 Å for WT/KNI-10033, I50V/KNI-10033, and I84V/KNI-10033, respectively, with a deviation of lower than 0.17 Å from the mean. On the other hand, RMSDs of 1.17, 1.22, and 1.28 Å are obtained for the inhibitor KNI-10075 when bound to PR_{WT}, PR_{I50V}, and PR_{I84V}, respectively. It may appear that there is a drift in the average RMSD during the initial 4 ns of the simulations. However, this drift is comparable to the fluctuations in the RMSD and in this sense not significant. For instance, the average RMSDs for KNI-10075 bound to the wild-type protease during the initial 4 ns and final 6 ns are 1.13 (±0.10) and 1.19 (±0.12) Å, respectively. A similar result was obtained for other cases also.

RMSD analyses were also performed for the flap regions of all complexes, with selected residues 44−55 and 44′−55′ (see Figure 4). Here, only the results for KNI-10075 complexed with wild-type and mutant variants are discussed. It is evident from Figure 4 that the mutations do not cause any change in

dx.doi.org/10.1021/jp3085292 | J. Phys. Chem. B 2013, 117, 5793−5805

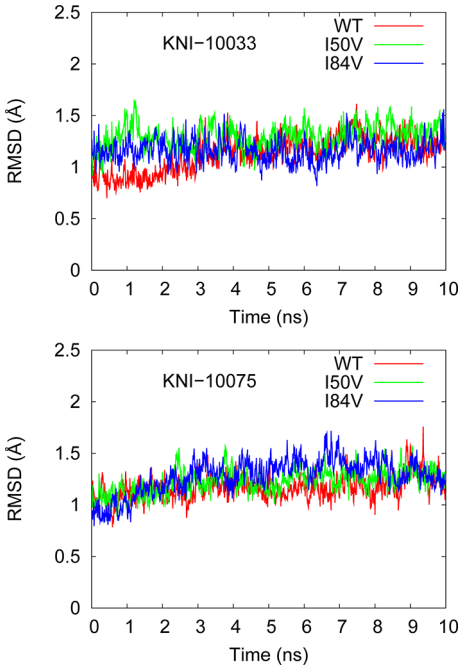

Figure 3. Time evolution of root-mean-square deviations (RMSDs) of backbone atoms relative to their initial configurations for wild-type (WT) and two mutant (I50V and I84V) proteases complexed with two different inhibitors, KNI-10033 (top) and KNI-10075 (bottom).

Table 2. Average RMSD during the 10 ns Production Simulations of the Protease−Inhibitor Complexes in Å and Standard Errors of the Mean (SEM) in Å

inhibitor	variant	RMSD	SEM
KNI-10033	WT	1.12	0.17
	I50V	1.30	0.12
	I84V	1.16	0.11
KNI-10075	WT	1.17	0.12
	I50V	1.22	0.12
	I84V	1.28	0.17

the RMSD for residues 44′−55′. However, a higher RMSD is observed for residues 44−55 of the I50V mutant complex compared to the wild-type and the I84V mutant.

Next, we determined the RMSD for the residues at the active site of the protease (see Figure 5). It is evident from this figure that mutations do not cause large structural changes. Subsequently, we performed an RMSD analysis of a region surrounding the active site. The area defined by residues 79−83 (and 79′−83′) covers the active site and comes in contact with the solvent. As shown in Figure 6, no large differences between these two regions of the protease were observed. Mutations cause no deviation for this region from the wild-type. The trend in RMSD for these regions shows similarities with previous observations in other HIV-1 PR−ligand complexes studied by Zoete et al.[55] and Tzoupis et al.[56]

A measure for the flexibility of the individual residues are the corresponding B-factors. The estimated B-factors of the individual residues for PR and its mutant variants complexed with the inhibitors are shown in Figure 7. Overall, the B-factor values for all complexes are quite similar. This may indicate that different ligands may not lead to significant conformational changes of the PR upon binding. Particularly small B-factors are observed for the catalytic dyad (3.23−3.36 Å^2 for Asp25 and

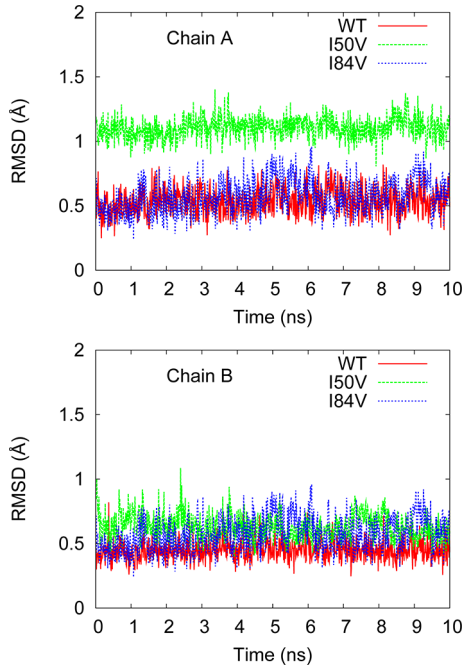

Figure 4. Time evolution of RMSD for residues 44−55 (chain A) or 44′−55′ (chain B) in the flap regions for KNI-10075 complexed with wild-type and mutant proteases.

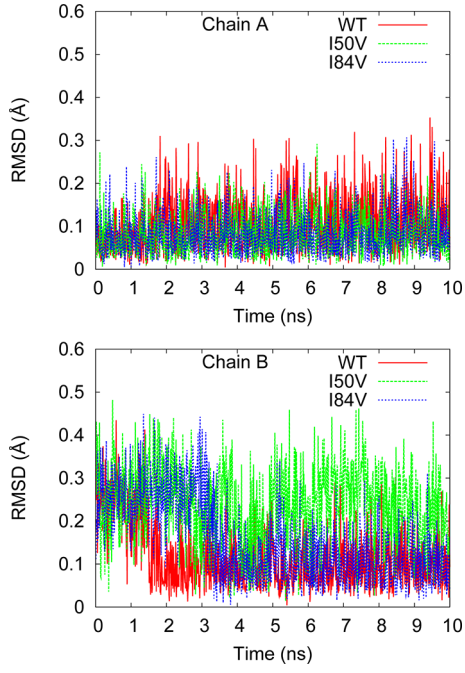

Figure 5. Time evolution of RMSD for active site residues Asp25−Thr26−Gly27 (chain A) or Asp25′−Thr26′−Gly27′ (chain B) for KNI-10075 complexed with wild-type and mutant proteases.

3.46−3.50 Å^2 for Asp25′) for all three complexes. This is expected, as the catalytic function of these residues presumably requires a well-defined stable three-dimensional structure.

As seen from Figure 7, the regions around 17(17′), 40(40′), 65(65′), and 99 show the biggest dynamic fluctuations, i.e., large B-factors. In the case of HIV-1 PR, the flexibility of the flap region is crucial for the activity of the protease. As seen from Figure 7, the flap region, especially the flap elbow region (37−42), shows significant flexibility. In an earlier study, a

dx.doi.org/10.1021/jp3085292 | J. Phys. Chem. B 2013, 117, 5793−5805

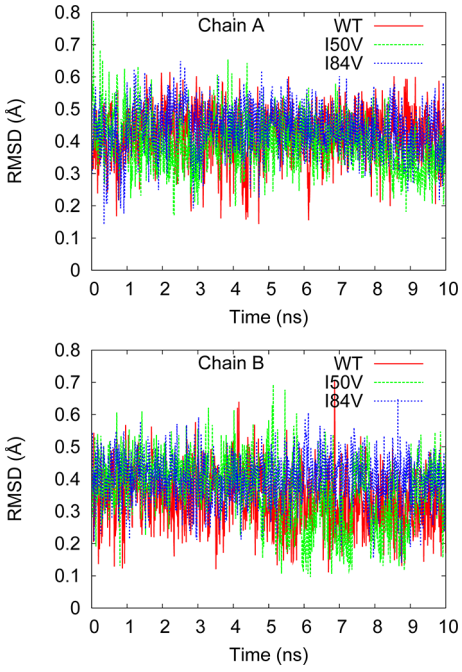

Figure 6. Time evolution of RMSD distribution for residues 79−83 (chain A) or 79′−83′ (chain B) for KNI-10075 complexed with wild-type and mutant proteases.

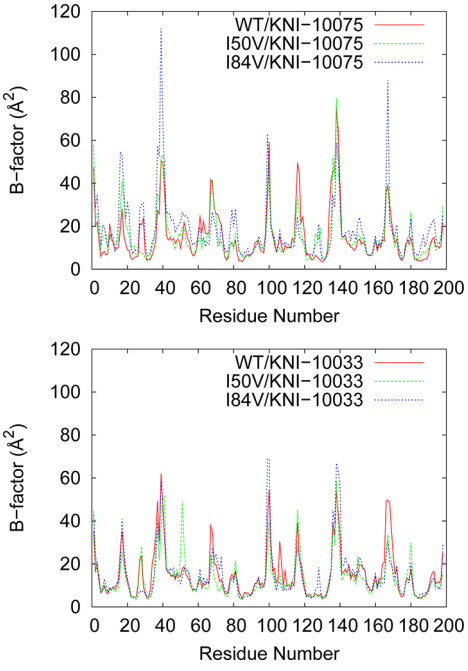

Figure 7. B-factors for HIV-1 protease and its mutant variants complexed with KNI-10033 and KNI-10075. Residues 1−99 and 100−198 correspond to residues 1−99 and 1′−99′, respectively.

similar behavior was observed for HIV-1 PR bound to other ligands.[33,34,57,58] For the PR_{I84V}−KNI 10075 complex, the regions around 40 and 65′ are more flexible compared to PR_{WT}−KNI 10075.

Figure S1 and S2 (see the Supporting Information) compare B-factors from our simulations with the experimental values for both ligands bound to the wild-type protease. Because no crystal structures of mutant complexes are available, we do not have any experimental B-factors for mutants to compare with simulated values. We observe trends in B-factors that are similar to those found experimentally. It is worth mentioning that the simulated B-factors correspond to a protein in solution, whereas the experimental values refer to a crystal.

Analysis of Active Site−Flap Distances. Concerning the local structural differences between WT and mutant HIV-1 PR, the flap movement is particularly important to explore. It is well-known that flap dynamics affect both the inhibitor binding and enzyme catalysis of HIV-1 PR. Moreover, several mutations affect flap dynamics. For example, L90M and V82F/I84V mutations open the flap a bit more in the mutant compared to the WT,[59] whereas the M46I mutation makes the flap more closed.[58] However, for the sameV82F/I84V double mutant, Hou and Yu[45] noticed that the flaps of the mutated protease and the wild-type protease possess similar dynamical properties and opening extent. In order to investigate the extent of flap opening in our MD simulations, the distance between the flap tip (I50 and I50′) and the catalytic Asp residues (D25 and D25′) was calculated. The results are depicted in Figure 8. The I50−D25 or I50′−D25′ distance (the distance between the C_α of I50/I50′ and that of D25/D25′) was believed to be a more appropriate measure for the flap opening than the tip−tip (I50−I50′) distance, because the tip−tip distance can be affected by both flap tip curling and flap asymmetry.[59]

It is clearly evident from Figure 8 that the distance between the flap tips and the active site did not change significantly upon mutation for chain B for all six complexes. On the other hand, for chain A, the distance between the flap tips and the active site is increased for I50V, while no change is observed for I84V.

3.3. Binding Mechanism for Calculated Protonation State. In our current study, we are interested to evaluate the relative potency of KNI-10033 and KNI-10075 against the wild-type and the mutant HIV-1 proteases and the molecular basis of possible drug resistance. In order to elucidate the binding mechanisms, we also determine the individual contributions to the binding free energies. Here, the contribution from the van der Waals or electrostatic interactions between the protease and the inhibitor, ΔE_{elec} or ΔE_{vdW}, the polar or nonpolar solvation free energy, ΔG_{pol} or ΔG_{np}, the sum of ΔE_{elec} and ΔG_{pol} denoted by $\Delta G_{pol,elec}$, as well as the contribution from the configurational entropy of the binding partners, denoted by $-T\Delta S_{MM}$, were considered.

Energetic Components. The energetics underlying the binding of KNI-10033 and KNI-10075 to the wild-type PR and its single mutant variants obtained from MM-PBSA calculations are shown in Table 3. The total binding free energies are found to have values between −5.6 and −19.5 kcal/mol for all PR−inhibitor complexes. The contributions favoring binding are the van der Waals interaction between the binding partners, being in the range −71.8 to −84.5 kcal/mol, and the intermolecular electrostatic interactions in the range −54.8 to −70.2 kcal/mol for all protease−inhibitor complexes. The nonpolar interactions with the solvent including the contribution from the hydrophobic effect yield contributions in the range −8.5 to −8.8 kcal/mol for KNI-10033 and KNI-10075 complexed with the wild-type and the mutant variants of the protease. Association is opposed by an unfavorable desolvation of polar groups, yielding a contribution of 99.7−112.6 kcal/mol for binding of KNI-10033 and KNI-10075 to the wild-type and mutant PR. As found for other systems,[16,32,60] the favorable intermolecular electrostatic interactions for the protease−inhibitor complexes in the gas phase are over-

dx.doi.org/10.1021/jp3085292 | J. Phys. Chem. B 2013, 117, 5793−5805

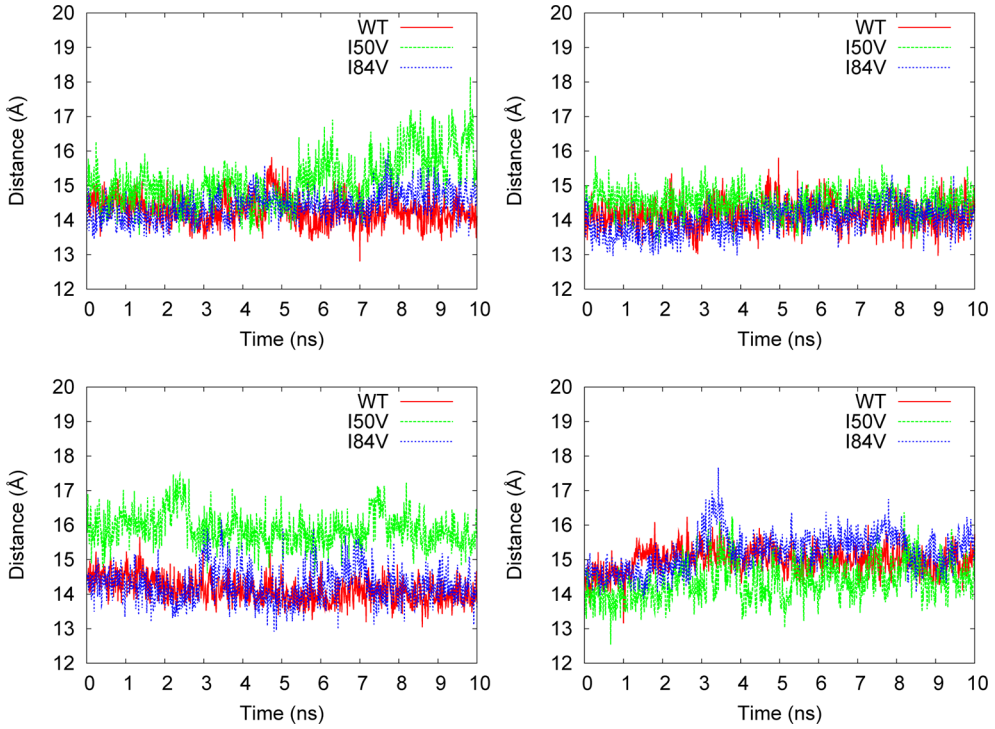

Figure 8. Time evolution of (top left) the D25−I50 C_a distances and (top right) the D25′−I50′ distances for KNI-10033 complexed with WT and mutants as well as (bottom left) the D25−I50 C_a distances and (bottom right) the D25′−I50′ distances for KNI-10075 bound to WT and mutants.

Table 3. Free Energy Terms (kcal/mol) for HIV-1 PR Variants Binding to Inhibitors KNI-10033 and KNI-10075[a]

PI	variant	ΔE_{elec}	ΔE_{vdW}	ΔG_{np}	ΔG_{pol}	ΔG_{solv}[b]	$\Delta G_{pol,elec}$[c]	$-T\Delta S$	ΔH[d]	ΔG_{bind}	ΔG^{exp}_{bind}
KNI-10033	WT	−61.7(0.3)	−84.5(0.2)	−8.7(0.01)	107.5(0.2)	98.8(0.2)	45.8(0.4)	31.6(0.4)	−47.4	−15.8(0.5)	−14.9
	I50V	−61.6(0.3)	−71.8(0.2)	−8.6(0.01)	101.8(0.3)	93.2(0.3)	40.2(0.4)	34.4(0.5)	−40.0	−5.6(0.5)	
	I84V	−56.7(0.3)	−82.7(0.2)	−8.7(0.01)	99.7(0.2)	91.0(0.2)	43.0(0.4)	28.9(0.6)	−48.4	−19.5(0.7)	
KNI-10075	WT	−54.8(0.3)	−83.2(0.1)	−8.5(0.01)	101.6(0.2)	93.1(0.3)	46.8(0.3)	28.3(0.5)	−44.9	−15.5(0.6)	−14.6
	I50V	−70.2(0.4)	−75.8(0.2)	−8.8(0.01)	112.6(0.3)	103.8(0.3)	42.4(0.4)	32.3(0.4)	−42.2	−9.9(0.6)	
	I84V	−59.2(0.3)	−79.1(0.2)	−8.7(0.01)	105.2(0.2)	96.5(0.2)	46.0(0.4)	27.5(0.6)	−41.8	−14.3(0.7)	

[a]Standard errors of the mean are given in parentheses. [b]$\Delta G_{solv} = \Delta G_{np} + \Delta G_{pol}$. [c]$\Delta G_{pol,elec} = \Delta G_{pol} + \Delta E_{elec}$. [d]$\Delta H = \Delta G_{solv} + \Delta E_{elec} + \Delta E_{vdW}$.

compensated by the unfavorable desolvation of polar groups. The sum of the contribution from the desolvation of polar groups and the intermolecular electrostatic interactions, $\Delta G_{pol,elec}$, is unfavorable to binding interactions, and varies from 40.2 to 46.8 kcal/mol for the protease−inhibitor complexes. A similar trend was found in our earlier studies of protease−inhibitor complexes.[33,34]

Configurational Entropy. Formation of macromolecular complexes is in general opposed by a loss in configurational entropy of the binding partners.[32−34,60,61] The restriction of a small molecule's motion on binding to a protein causes a loss of configurational entropy, and thus a penalty in binding affinity. The protein contribution could be especially important for HIV protease, where binding is associated with a marked reduction in the mobility of the active site flaps; significant coupling of protein and ligand motions also is expected.[62] The corresponding loss in entropy due to the translational, rotational, and vibrational degrees of freedom made free energy contributions between 27.5 and 34.4 kcal/mol for all protein−inhibitor complexes.

It should be noted that some effects which are entropic in experiment like those coming from (de)hydation (hydrophobic and electrostatic effects) are not explicitly entropic in our calculations but included in the solvation terms (for which entropy and enthalpy are not distinguished). However, ΔG_{solv} may also formally be decomposed into an enthalpic and an entropic term if the temperature dependence of the dielectric permittivity is considered.[63] It should be emphasized that we are interested in the influence of configurational entropy of the binding partners (or solutes) only. Hence, this decomposition was not performed.

PR_{WT}/KNI-10033 versus PR_{WT}/KNI-10075. The experimental binding free energies for KNI-10033 and KNI-10075 are −14.9 and −14.6 kcal/mol, respectively,[7] in good agreement with the calculated binding free energies, which are found to be −15.8 (±0.5) and −15.5 (±0.6) kcal/mol, respectively. For both complexes, the complex formation is favored by the intermolecular electrostatic and van der Waals interactions as well as the nonpolar component of the solvation free energy and these components are more favorable for PR/KNI-10033 compared to PR/KNI-10075. If the configurational entropy is not considered, the binding free energy is more favorable for the PR/KNI-10033 complex than for PR/KNI-10075 by −2.5 kcal/mol. However, both ligands possess a similar binding free energy against the wild-type PR. This is because the contribution from the configurational entropy which disfavors the complex formation is less unfavorable in the case of PR/KNI-10075 compared to PR/KNI-10033 by 3.3 kcal/mol.

dx.doi.org/10.1021/jp3085292 | J. Phys. Chem. B 2013, 117, 5793−5805

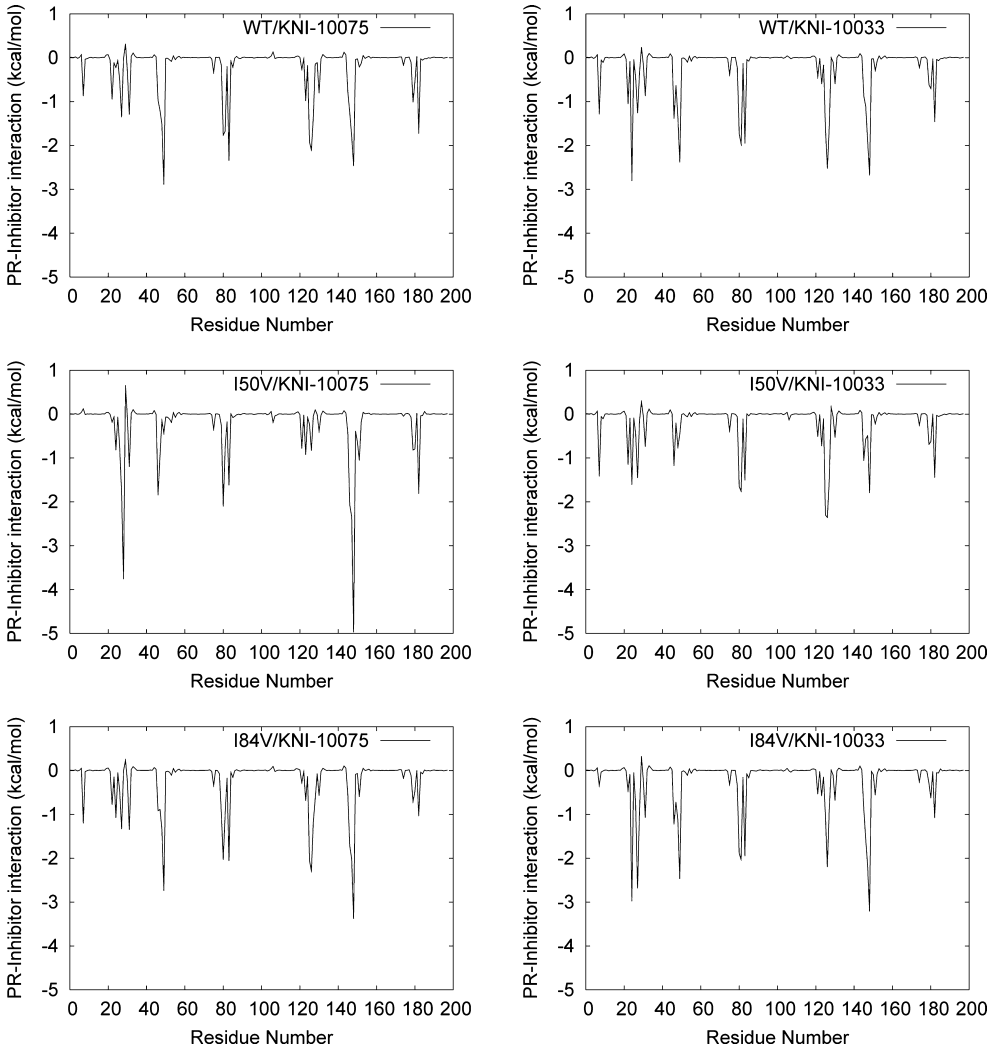

Figure 9. Decomposition of ΔG into contributions from individual residues for the protease−inhibitor complexes. Residues 1−99 correspond to chain A and residues 100−198 to chain B of the protease. The lack of symmetry between the two monomers arises due to the presence of ligand.

3.4. Mutation Induced Shifts in Affinity. The mechanism underlying the mutation-induced changes in affinity may be elucidated from the variation of different components of the binding free energy upon mutations shown in Table 3. As given in the table, the predicted total binding free energies of the WT, PR_{I50V}, and PR_{I84V}/KNI-10033 complexes are −15.8, −5.6, and −19.7 kcal/mol, respectively. Corresponding binding free energies of the WT, PR_{I50V}, and PR_{I84V}/KNI-10075 complexes are −15.5, −9.9, and −14.3 kcal/mol, respectively.

Compared to the PR_{WT}−KNI-10033 complex, the mutants PR_{I50V} and PR_{I84V} caused shifts in the binding free energy by 10.2 and −3.6 kcal/mol, respectively. These values suggest that the I50V mutant binds less strongly to KNI-10033. This decrease in the size of the binding free energy correlates with unfavorable shifts in (i) the van der Waals interactions ΔE_{vdW} by 12.7 kcal/mol and (ii) the configurational entropy by 2.8 kcal/mol. The changes in the contributions from the desolvation of nonpolar groups ΔG_{np} and the intermolecular electrostatic interactions ΔE_{elec} are almost zero. The polar solvation free energy ΔG_{pol} is less unfavorable relative to the wild-type, being shifted by −5.7 kcal/mol. However, this change in ΔG_{pol} is not sufficient to compensate for the loss in ΔE_{vdW} causing drug resistance. On the other hand, the I84V mutant does not cause any drug resistance. Rather, the inhibitor is more potent against PR_{I84V} compared to PR_{WT}. Unfavorable shifts in ΔE_{elec} and ΔE_{vdW} are overcompensated by favorable changes in ΔG_{pol} and entropy, leading to an improved affinity relative to the wild-type protease.

In contrast to KNI-10033, the inhibitor KNI-10075 shows drug resistance against both I50V and I84V. The binding free energies are shifted by 5.6 or 1.2 kcal/mol relative to the wild-type case for PR_{I50V} or PR_{I85V}/KNI-10075, respectively. For the PR_{I50V}−KNI-10075 complex, ΔE_{elec} is changed by −15.4 kcal/mol compared to the wild-type. This favorable shift in ΔE_{elec}, however, is overcompensated by unfavorable changes in ΔE_{vdW}, ΔG_{pol}, and entropy by 7.4, 11.0, and 4.0 kcal/mol, respectively, which leads to a reduced potency against PR_{I50V}. On the other hand, we see a marginal loss in the size of the binding free energy for PR_{I84V}/KNI-10075 compared to the PR_{WT}/KNI-10075 complex due to unfavorable shifts in ΔE_{vdW} and ΔG_{pol}.

Contributions from Individual Residues to the Binding Free Energy. In order to gain a detailed picture of the basis of the potency due to the single point mutations, the binding free energy was further decomposed into contributions from individual residues to generate an inhibitor−residue interaction spectrum, as shown in Figure 9. This is extremely useful to understand the drug resistance mechanism of KNI-10033 and KNI-10075 to protease at the atomic level. From Figure 9, it is

dx.doi.org/10.1021/jp3085292 | J. Phys. Chem. B 2013, 117, 5793−5805

clear that the overall interaction spectra of all six complexes are quite similar. The attractive contributions mainly come from six groups around Ala28/Ala28′, Ile50/Ile50′, and Ile84/Ile84′. The positions of these residues in the complex are shown in Figure 10.

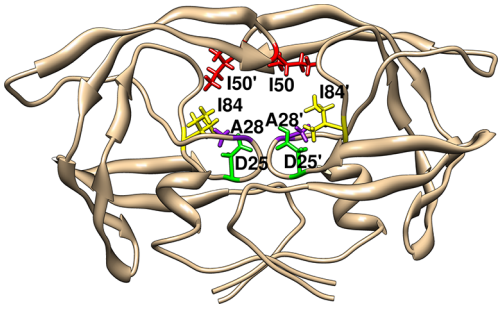

Figure 10. Important protease residues that contribute significantly to the binding free energies are shown in stick representation.

Table 4 reports the decomposition of ΔG_{bind} on a per-residue basis into contributions from van der Waals and electrostatic interactions, as well as polar and nonpolar solvation energies for residues with $|\Delta G| \geq 1.5$ kcal/mol for the three complexes. The decomposition of ΔG_{bind} was carried out using the MM-GBSA scheme. For all listed residues, the van der Waals energy and nonpolar solvation energy drive the binding of the inhibitors to PR. The most significant contributions to the binding free energy come from Asp25 (−2.8 kcal/mol), Ala28′ (−2.4 kcal/mol), and Ile50′ (−3.2 kcal/mol) for PR_{WT}, PR_{I50V}, and PR_{I84V}/KNI-10033, respectively. Most of the contributions of Ala′ of PR_{WT}/KNI-10033 and Ile50′ of PR_{I84V}/KNI-10033 derive from the van der Waals interactions. For Asp25, most of the contributions come from the intermolecular electrostatic interactions. For Asp25 and Ile50′, the side chain contributes more favorably than the backbone and the contributions from the side chain are −2.8 or −2.6 kcal/mol for PR_{WT}/KNI-10033 or PR_{I84V}/KNI-10033, correspondingly. On the other hand, for Ala28′ of PR_{I50V}/KNI-10033, the backbone contributes more favorably than the side chain and the contribution from the backbone is −1.5 kcal/mol.

For PR_{WT}/KNI-10075, the most significant contributions come from Ile50 (−2.9 kcal/mol). In the case of PR_{I50V}/KNI-10075 or PR_{I84V}/KNI-10075, the most significant contributions come from Val50′ (−5.0 kcal/mol) or Ile50′ (−3.4 kcal/mol), respectively, and most of the contributions derive from the electrostatic or van der Waals interactions, correspondingly. For both Val50′ and Ile50′, the side chain contributes more favorably than the backbone. Similar to Val′, most of the contribution of Ile50 comes from the side chain. Gly49′ also provides large contributions to the binding free energy varying in the range −1.8 to −2.3 kcal/mol. Most of the contributions originate from the electrostatic interactions for I50V and I84V or from the van der Waals interactions for WT/KNI-10075.

Contribution of Aspartic Dyad to Binding Free Energies. The catalytic aspartic dyad Asp25/Asp25′ is expected to be crucial for the binding of the inhibitors to the protease. Hence, it is important to estimate the total contribution from the Asp25 dyad to the binding free energy. The contributions from Asp25/Asp25′ to the binding free energies are provided in Table 5. We found the total contribution from Asp25/Asp25′ to be attractive, varying in the range −1.2 to −3.5 kcal/mol for all PR−inhibitor complexes. For all six complexes, both Asp25 and Asp25′ contributed favorably to the binding free energy. The total contributions of the Asp25 dyad to the binding free energies were always more favorable for PR−KNI-10033 compared to the PR−KNI-10075 complexes. Asp25 always contributed more favorably than Asp25′ for KNI-10033 in complex with the wild-type or mutant PR. However, the opposite was observed for KNI-10075 bound to the wild-type or I50V mutant, while a similar trend was observed for the PR_{I84V}−KNI-10075 complex. The total contribution of Asp25/Asp25′ was the most favorable in the case of PR_{I84V}−KNI-10033 (−3.5 kcal/mol) and the least favorable for PR_{WT}−KNI-10075 (−1.2 kcal/mol).

The individual contributions from the two Asp residues to the binding free energy are described in the following. For the PR_{WT}−KNI-10033 complex, both Asp25 and Asp25′ contributed favorably and the contribution from Asp25 (−2.9 kcal/mol) was more than 4 times that of Asp25′ (−0.6 kcal/mol). For PR_{I50V}−KNI-10033, the contribution from Asp25 (−1.6 kcal/mol) was twice the contribution from Asp25′, while a 5 times more favorable contribution was observed for Asp25 (−3.0 kcal/mol) compared to Asp25′ for PR_{I84V}−KNI-10033. For the PR_{WT}−KNI-10075 complex, Asp25′ yielded a favorable contribution of −1.0 kcal/mol, which was 5 times the contribution from Asp25′ (−0.2 kcal/mol), while a similar contribution from both residues was observed for PR_{I50V}−KNI-10075. On the other hand, Asp25 yielded a more favorable contribution (−1.1 kcal/mol) than Asp25′ for the PR_{I84V}−KNI-10075 complex.

3.5. Interactions Governing Binding of KNI-10033 and KNI-10075 to PR versus Darunavir and GRL-06579A to PR. To study the difference in binding mechanisms between KNI-10033 or KNI-10075 and darunavir (DRV) or GRL-06579A complexes, the individual contributions to the respective shifts, $\Delta\Delta E_{elec}$, $\Delta\Delta E_{vdW}$, and so forth, were computed (see Table 6). Recently, two of us[34] have studied the binding of darunavir and GRL-06579A to HIV-1 protease. For the comparison of the energetics of PR−KNI-10033 or PR−KNI-10075 and PR−DRV or PR−GRL-06579A, the values for DRV and GRL-06579A were taken from that earlier study.[34] KNI-10033, KNI-10075, and DRV show similar affinities, while GRL-06579A is more potent compared to KNI-10033 and KNI-10075. It should be noted here that the experimental binding free energies for DRV and GRL-06579A are −15.1 and −17.0 kcal/mol, respectively, in good agreement with the calculated values −15.7 (±0.5) and −17.5 (±0.6) kcal/mol, respectively.[34]

PR_{WT}−KNI-10033 versus PR_{WT}−DRV. Darunavir and KNI-10033 have similar binding affinities for wild-type PR. It would be interesting to compare the binding mechanism between these two inhibitors. In both cases, the intermolecular electrostatic and van der Waals interactions as well as the nonpolar solvation free energies contributed favorably to the complex formation. However, these three terms are more favorable in the case of PR−KNI-10033 relative to PR−DRV. For the former, the gas phase electrostatic and van der Waals interactions are shifted by −7.5 and −20.5 kcal/mol, respectively, compared to PR−DRV. There is also a favorable change in the nonpolar solvation free energy which is shifted by −2.0 kcal/mol relative to PR−DRV. However, the polar solvation free energy which disfavors the complex formation, is less unfavorable in the case of PR−DRV compared to PR−KNI-10033. For the latter, the polar solvation free energy is increased by 26.3 kcal/mol and the entropic contribution by 3.8

dx.doi.org/10.1021/jp3085292 | J. Phys. Chem. B 2013, 117, 5793−5805

Table 4. Decomposition of Binding Free Energies ΔG for the PR−Inhibitor Complexes into Contributions from Individual Residues[a]

residue	T_{vdW}	T_{ele}	T_{GB}	T_{np}	T_S	T_B	T_{TOT}
			WT/KNI-10033				
Asp25	−0.1	−8.7	6.0	−0.1	−2.8	−0.1	−2.9
Ile50	−2.2	−1.3	1.3	−0.2	−2.0	−0.4	−2.4
Pro81	−1.5	−0.3	0.4	−0.3	−1.4	−0.3	−1.7
Val82	−1.8	0.1	−0.1	−0.2	−1.7	−0.3	−2.0
Ile84	−1.9	−0.1	0.2	−0.2	−1.9	−0.1	−2.0
Gly27′	−1.6	−1.5	1.6	−0.2	−0.2	−1.5	−1.6
Ala28′	−2.1	−1.0	0.8	−0.2	−0.9	−1.6	−2.5
Asp29′	−1.2	−3.9	3.6	−0.1	−0.1	−1.5	−1.6
Gly49′	−1.8	−2.1	2.2	−0.2	−0.6	−1.3	−1.9
Ile50′	−2.9	−1.5	1.9	−0.2	−2.3	−0.4	−2.7
			I50V/KNI-10033				
Asp25	−0.2	−11.8	10.5	−0.1	−1.5	−0.1	−1.6
Pro81	−1.5	−0.3	0.4	−0.3	−1.2	−0.5	−1.7
Val82	−1.6	−0.1	0.1	−0.2	−1.6	−0.2	−1.8
Ile84	−1.4	0.2	−0.1	−0.2	−1.4	−0.1	−1.5
Gly27′	−1.9	−3.0	2.8	−0.2	−0.1	−2.2	−2.3
Ala28″	−2.1	−1.3	1.2	−0.2	−0.9	−1.5	−2.4
Asp29′	−1.2	−2.8	2.6	−0.1	−0.02	−1.5	−1.5
Val50′	−2.0	−1.0	1.4	−0.2	−1.4	−0.4	−1.8
			I84V/KNI-10033				
Asp25	−0.2	−6.3	3.6	−0.1	−2.9	−0.1	−3.0
Ala28	−2.3	−0.8	0.5	−0.1	−0.9	−1.8	−2.7
Ile50	−2.3	−1.0	1.1	−0.3	−2.1	−0.4	−2.5
Pro81	−1.6	−0.3	0.4	−0.4	−1.5	−0.4	−1.9
Val82	−1.7	0.1	−0.1	−0.3	−1.7	−0.3	−2.0
Val84	−1.6	−0.1	−0.1	−0.2	−1.6	−0.4	−2.0
Ala28′	−2.0	−0.4	0.4	−0.2	−0.9	−1.3	−2.2
Gly48′	−1.5	−2.8	3.0	−0.2	−0.0	−1.5	−1.5
Gly49′	−2.0	−2.5	2.5	−0.2	−0.4	−1.8	−2.2
Ile50′	−3.3	−1.9	2.2	−0.2	−2.6	−0.6	−3.2
			WT/KNI-10075				
Gly49	−1.3	−2.0	1.9	−0.1	−0.2	−1.3	−1.5
Ile50	−2.9	−1.7	1.9	−0.2	−2.4	−0.5	−2.9
Pro81	−1.6	−0.4	0.5	−0.3	−1.4	−0.4	−1.8
Val82	−1.5	−0.0	0.0	−0.2	−1.5	−0.2	−1.7
Ile84	−2.2	−0.1	0.1	−0.2	−2.2	−0.2	−2.4
Gly27′	−1.9	−2.0	2.2	−0.2	−0.1	−1.8	−1.9
Ala28′	−2.2	−0.5	0.7	−0.1	−0.9	−1.2	−2.1
Gly49′	−1.8	−1.4	1.6	−0.2	0.0	−1.8	−1.8
Ile50′	−2.5	−0.3	0.5	−0.2	−2.0	−0.5	−2.5
Ile84′	−1.6	−0.3	0.3	−0.1	−1.6	−0.1	−1.7
			I50V/KNI-10075				
Ala28	−1.7	−0.5	0.5	−0.1	−0.5	−1.3	−1.8
Asp29	−1.3	−12.1	9.9	−0.3	−3.3	−0.5	−3.8
Ile47	−1.7	−0.6	0.6	−0.2	−1.5	−0.4	−1.9
Pro81	−1.9	−0.5	0.5	−0.2	−1.8	−0.3	−2.1
Ile84	−1.9	−0.5	0.6	0.2	−1.5	−0.1	−1.6
Gly48′	−1.8	−3.4	3.4	−0.3	−0.3	−1.8	−2.1
Gly49′	−2.0	−2.5	2.3	−0.1	0.1	−2.4	−2.3
Val50′	−3.2	−4.1	2.7	−0.4	−2.7	−2.3	−5.0
Ile84′	−1.7	−0.2	0.2	−0.1	−1.7	−0.1	−1.8
			I84V/KNI-10075				
Ile50	−1.7	−0.2	0.2	−0.1	−2.1	−0.7	−2.8
Pro81	−1.9	−0.5	0.4	−0.2	−1.7	−0.3	−2.0
Val84	−1.58	0.05	−0.09	−0.14	−1.71	−0.35	−2.1
Gly27′	−1.2	−0.6	−0.1	−0.2	−0.1	−2.0	−2.1
Ala28′	−2.4	−1.9	0.5	−0.2	−0.8	−1.5	−2.3
Gly48′	−1.3	−1.7	1.5	−0.2	−0.1	−1.6	−1.7
Gly49′	−1.4	−1.8	1.5	−0.3	−0.4	−1.6	−2.0

dx.doi.org/10.1021/jp3085292 | J. Phys. Chem. B 2013, 117, 5793−5805

Table 4. continued

residue	T_{vdW}	T_{ele}	T_{GB}	T_{np}	T_S	T_B	T_{TOT}
			I84V/KNI-10075				
Ile50′	−2.4	−1.2	1.1	−0.1	−2.5	−0.9	−3.4

[a]The contributions from the van der Waals (T_{vdW}) and electrostatic interactions (T_{ele}) as well as the polar (T_{GB}) and nonpolar solvation energy (T_{np}) and the total contribution of a given residue (T_{TOT}) are shown. T_S and T_B represent the backbone and side chain contributions. Only residues with $|\Delta G| \geq 1.5$ kcal/mol are listed. All values are given in kcal/mol. The standard errors of the free energy estimates as well as of individual components are not larger than 0.4 kcal/mol.

Table 5. Contribution of the Asp25 Dyad to the Binding Free Energy[a]

inhibitor	variant	Asp25	Asp25′	total
KNI-10033	WT	−2.9(0.3)	−0.6(0.2)	−3.5(0.4)
	I50V	−1.6(0.3)	−0.7(0.2)	−2.3(0.4)
	I84V	−3.0(0.1)	−0.6(0.2)	−3.6(0.2)
KNI-10075	WT	−0.2(0.3)	−1.0(0.2)	−1.2(0.4)
	I50V	−0.9(0.3)	−0.9(0.2)	−1.8(0.4)
	I84V	−1.1(0.3)	−0.7(0.2)	−1.8(0.4)

[a]Values are given in kcal·mol^{-1}. Standard errors of the mean are given in parentheses.

kcal/mol relative to PR−DRV. For PR−KNI-10033, the total gain in the intermolecular electrostatic and van der Waals interactions as well as the nonpolar solvation free energy is compensated by an increase in the polar solvation free energy, leading to a similar affinity for both ligands.

PR_{WT}−KNI-10075 versus PR_{WT}−DRV. Experimentally, DRV and KNI-10075 show a similar affinity for HIV-1 PR in agreement with our calculations. Comparing the components of the binding free energy of PR1−KNI-10075 and PR−DRV gives insights into the difference in the binding mechanisms. For PR−KNI-10075, the nonpolar solvation free energy ΔG_{np} and the van der Waals interaction energy ΔE_{vdW} are more favorable than those for PR−DRV, being shifted by −2.0 and −19.2 kcal/mol, respectively, compared to the latter. The intermolecular electrostatic energy ΔE_{elec} is similar for both complexes. However, the polar solvation free energy, which unfavors the complex formation, is less unfavorable for PR−DRV compared to PR−KNI-10075. For the PR−DRV complex, the polar solvation free energy is shifted by −20.4 kcal/mol compared to PR−KNI-10075. The increase in the size of the intermolecular van der Waals interaction energy ΔE_{vdW} for PR−KNI-10075 is thus countered by the increase in the polar solvation free energy ΔG_{pol}. Hence, DRV and KNI-10075 show similar affinities for PR.

PR_{WT}−KNI-10033 versus PR_{WT}−GRL-06579A. In both cases, the intermolecular electrostatic and van der Waals interactions as well as the nonpolar solvation free energies contributed favorably to the complex formation. However, these three terms are more favorable in the case of PR−KNI-10033 compared to PR−GRL-06579A. From this, it would be expected that KNI-10033 is more potent against HIV-1 PR than GRL-06579A. In contrast, GRL-06579A is more potent against HIV-1 PR than KNI-10033. For the latter, the gas phase electrostatic and van der Waals interactions are shifted by −9.4 and −17.9 kcal/mol, and the nonpolar solvation free energy is changed by −2.2 kcal/mol relative to PR−GRL-06579A. However, the polar solvation free energy, which disfavors the complex formation, is less unfavorable in the case of PR−GRL-06579A compared to PR−KNI-10033. For the latter, the polar solvation free energy is increased by 26.5 kcal/mol and the entropy is shifted by 4.5 kcal/mol relative to PR−GRL-06579A. The total gain in the size of ΔE_{elec}, ΔE_{vdW}, and ΔG_{np} is compensated by the increase in the polar solvation free energy and entropy, leading to a similar affinity for both ligands. The increase in potency for GRL-06579A compared to KNI-10033 is mainly due to a decrease in ΔG_{pol} relative to KNI-10033.

PR_{WT}−KNI-10075 versus PR_{WT}−GRL-06579A. The PR_{WT}−KNI-10075 complex has a somewhat lower affinity than PR_{WT}−GRL-06579A; the corresponding shift in the binding free energy of +2.0 kcal/mol is in agreement with the experimental value of +2.4 kcal/mol. GRL-06579A shows weaker van der Waals and intermolecular electrostatic interactions with PR than KNI-10075 with PR_{WT}, which are shifted by −16.6 and −2.5 kcal/mol, respectively. The nonpolar solvation free energy is less favorable for PR_{WT}−GRL-06579A than for PR_{WT}−KNI-10075 by −1.8 kcal/mol. On the other hand, the contribution from the desolvation of polar groups is less unfavorable for PR_{WT}−GRL-06579A compared to PR_{WT}−KNI-10075 by 26.5 kcal/mol. The net contribution from polar interactions to the binding free energy is more favorable for PR_{WT}−GRL-06579A than for PR_{WT}−KNI-10075 by 24.0 kcal/mol. Hence, due to the lower polar solvation free energy, GRL-06579A retains more potency against HIV-1 PR than KNI-10075.

4. CONCLUSION

In the present work, we have studied the binding of HIV-1 PR_{WT}, PR_{I50V}, and PR_{I84V} to KNI-10033 and KNI-10075 using a combination of 10 ns MD simulations in explicit water and implicit solvent free energy calculations. Experiments show that the I50V mutation causes drug resistance for darunavir,

Table 6. Free Energy Terms of PR−KNI-10033 and PR−KNI-10075 Relative to PR−DRV and PR−GRL-06579A in kcal/mol[a]

	KNI-10033		KNI-10075	
component	DRV	GRL-06579A	DRV	GRL-06579A
$\Delta\Delta E_{elec}$	−7.5(0.4)	−9.4(0.4)	−0.6(0.4)	−2.5(0.4)
$\Delta\Delta E_{vdW}$	−20.5(0.2)	−17.9(0.2)	−19.2(0.1)	−16.6(0.1)
$\Delta\Delta G_{np}$	−2.0(0.01)	−2.2(0.01)	−2.0(0.01)	−1.8(0.01)
$\Delta\Delta G_{pol}$	26.3(0.5)	26.5(0.2)	20.4(0.5)	26.5(0.2)
$-\Delta T\Delta S_{MM}$	3.8(0.6)	4.5(0.6)	0.5(0.6)	1.2(0.7)

[a]Standard errors of the mean are provided in parentheses.

dx.doi.org/10.1021/jp3085292 | J. Phys. Chem. B 2013, 117, 5793−5805

saquinavir,[64] and amprenavir.[65] This implies that this mutation (i) decreases the affinities of these drugs for the HIV-1 protease while (ii) it neither impairs the substrate binding nor the product unbinding process nor the interaction with the transition state of the enzymatic reaction. The effect (ii) which is independent of the drug, together with our result that the same mutation also significantly decreases the affinities of KNI-10033 and KNI-10075 for the protease, suggests that this mutation also causes drug resistance against the latter two inhibitors. Interestingly, I84V causes drug resistance against KNI-10075, while KNI-10033 is more potent against I84V compared to wild-type protease. The drug resistance arises mainly from the loss in the intermolecular van der Waals interaction energy. For PR_{I50V}−KNI-10075, an increased polar solvation free energy also plays a vital role in drug resistance. For the PR_{I84V}−KNI-10033 complex, favorable shifts in the polar solvation and the entropic contribution relative to the wild-type PR−KNI-10033 cause an increased potency. The latter results show that neglecting changes in configurational entropy in the computation of relative binding affinities as often done is not appropriate in general. On the other hand, for PR_{I84V}−KNI-10075, unfavorable shifts in the van der Waals interaction energy and polar solvation free energy lead to a decreased potency compared to PR_{WT}−KNI-10075. The importance of the polar solvation free energy is revealed when interactions governing binding of KNI-10033 or KNI-10075 to the wild-type protease are compared to the wild-type protease complexed with darunavir or GRL-06579A. An increase in the intermolecular electrostatic and van der Waals interactions as well as an increase in the nonpolar solvation free energy compared to darunavir or GRL-06579A are compensated by an increased polar solvation free energy, resulting in similar affinities. The importance of the polar solvation revealed here highlights that structural inspection alone is not sufficient for the understanding and the design of drugs but that solvation effects must be taken into account. Our results might assist in designing new antiretroviral drugs targeting HIV-1 protease.

■ ASSOCIATED CONTENT

Supporting Information

Figures S1 and S2 comparing B-factors obtained from simulations with experiment. This material is available free of charge via the Internet at http://pubs.acs.org.

■ AUTHOR INFORMATION

Corresponding Author

*E-mail: volker.knecht@physik.uni-freiburg.de. Phone: +49-761-203-5913. Fax: +49-761-203-5883.

Present Addresses

[†]P.K.: Department of Biochemistry & Molecular Biology, Michigan State University, 603 Wilson Road, East Lansing, MI 48824-1319, USA.

[‡]V.K.: Biomolecular Dynamics, Institute of Physics, Albert Ludwigs University, Hermann-Herder Straße 3, 79104 Freiburg, Germany.

Notes

The authors declare no competing financial interest.

■ ACKNOWLEDGMENTS

The work was supported by the Federal Ministry of Education and Research (BMBF), Germany. P.K. acknowledges the support from the German Research Foundation (DFG) in the framework of the International Graduate Research Training Group 1524 (IGRTG 1524).

■ REFERENCES

(1) Hornak, V.; Okur, A.; Rizzo, R. C.; Simmerling, C. *Proc. Natl. Acad. Sci. U.S.A.* **2006**, *103*, 915−920.
(2) Wood, E.; Hogg, R. S.; Yip, B.; Moore, D.; Harringan, P. R.; Montaner, J. S. *HIV Med.* **2007**, *8*, 80−85.
(3) Walker, B. D.; Burton, D. R. *Science* **2008**, *320*, 760−764.
(4) Foulkes-Murzycki, J. E.; Scott, W. R.; Schiffer, C. A. *Structure* **2007**, *15*, 225−233.
(5) Shafer, R. W.; Schapiro, J. M. *AIDS Rev.* **2008**, *10*, 67−84.
(6) Vergene, L.; Peeters, M.; Mpoudi-Ngole, E.; Bourgeois, A.; Liegeois, F.; Toure-Kane, C.; Mboup, S.; Mulanga-Kabeya, C.; Saman, E.; Jourdan, J.; et al. *J. Clin. Microbiol.* **2000**, *38*, 3919−3925.
(7) Lafont, V.; Armstrong, A. A.; Ohtaka, H.; Kiso, Y.; Amzel, L. M.; Freire, E. *Chem. Biol. Drug Des.* **2007**, *69*, 413−422.
(8) Clavel, F.; Hance, A. J. *N. Engl. J. Med.* **2004**, *350*, 1023−1035.
(9) Zwanzig, R. W. *J. Chem. Phys.* **1954**, *22*, 1420−1426.
(10) Kirkwood, J. G. *J. Chem. Phys.* **1935**, *3*, 300−313.
(11) Laio, A.; Parrinello, M. *Proc. Natl. Acad. Sci. U.S.A.* **2002**, *99*, 12562−12566.
(12) Torrie, G. M.; Valleau, J. P. *J. Comput. Phys.* **1977**, *23*, 187−199.
(13) Kollman, P. A.; Massova, I.; Reyes, C.; Kuhn, B.; Huo, S.; Chong, L.; Lee, M.; Lee, T.; Duan, Y.; Wang, W.; et al. *Acc. Chem. Res.* **2000**, *33*, 889−897.
(14) Jayaram, B.; Sprous, D.; Young, M. A.; Beveridge, D. L. *J. Am. Chem. Soc.* **1998**, *120*, 10629−10633.
(15) Vorobjev, Y. N.; Almagro, J. C.; Hermans, J. *Proteins* **1998**, *32*, 399−413.
(16) Kuhn, B.; Kollman, P. A. *J. Med. Chem.* **2000**, *43*, 3786−3791.
(17) Rastelli, G.; Rio, A. D.; Degliesposti, G.; Sgobba, M. *J. Comput. Chem.* **2010**, *31*, 797−810.
(18) Reyes, C. M.; Kollman, P. A. *J. Mol. Biol.* **2000**, *295*, 1−6.
(19) Reyes, C. M.; Kollman, P. A. *J. Mol. Biol.* **2000**, *297*, 1145−1158.
(20) Chen, X.; Weber, I. T.; Harrison, R. W. *J. Mol. Model.* **2004**, *10*, 373−381.
(21) Hou, T.; McLaughlin, W. A.; Wang, W. *Proteins* **2007**, *71*, 1163−1174.
(22) Wang, J.; Morin, P.; Wang, W.; Kollman, P. A. *J. Am. Chem. Soc.* **2001**, *123*, 5221−5230.
(23) Worch, R.; Bökel, C.; Höfinger, S.; Schwille, P.; Weidemann, T. *Proteomics* **2010**, *10*, 4196−4208.
(24) Kar, P.; Seel, M.; Weidemann, T.; Höfinger, S. *FEBS Lett.* **2009**, *583*, 1909−1915.
(25) Karplus, M.; Kushick, J. N. *Macromolecules* **1981**, *14*, 325−332.
(26) Rempe, S. B.; Jonsson, H. *Chem. Educ.* **1998**, *3*, 1−17.
(27) Duan, Y.; Wu, C.; Chowdhury, S.; Lee, M. C.; Xiong, G.; Zhang, W.; Yang, R.; Cieplak, P.; Luo, R.; Lee, T. *J. Comput. Chem.* **2003**, *24*, 1999−2012.
(28) Wang, J.; Wolf, R. M.; Caldwell, J. W.; Kollman, P. A.; Case, D. A. *J. Comput. Chem.* **2004**, *25*, 1157−1174.
(29) Jakalian, A.; Jack, D. B.; Bayly, C. I. *J. Comput. Chem.* **2002**, *23*, 1623−1641.
(30) Wang, J.; Wang, W.; Kollman, P. A.; Case, D. A. *J. Mol. Graphics Modell.* **2006**, *25*, 247−260.
(31) Case, D. A.; Cheatham, T. E.; Darden, T.; Gohlke, H.; Luo, R.; Merz, K. M., Jr.; A. Onufriev, A.; Simmerling, C.; Wang, B.; Woods, R. *J. Comput. Chem.* **2005**, *26*, 1668−1688.
(32) Kar, P.; Lipowsky, R.; Knecht, V. *J. Phys. Chem. B* **2011**, *115*, 7661−7669.
(33) Kar, P.; Knecht, V. *J. Comput.-Aided Mol. Des.* **2012**, *26*, 215−232.
(34) Kar, P.; Knecht, V. *J. Phys. Chem. B* **2012**, *116*, 2605−2614.
(35) Kar, P.; Knecht, V. *J. Phys. Chem. B* **2012**, *116*, 6137−6149.
(36) Kar, P.; Knecht, V. *J. Phys. Chem. B* **2012**, *116*, 6269−6278.
(37) Jorgensen, W. L.; Chandrasekar, J.; Madura, J. D.; Impey, R.; Klein, K. *J. Chem. Phys.* **1983**, *79*, 926−935.

(38) Ryckaert, J.-P.; Ciccotti, G.; Berendsen, H. J. C. *J. Comput. Phys.* **1977**, *23*, 327−341.
(39) Darden, T.; York, D.; Pedersen, L. *J. Chem. Phys.* **1993**, *98*, 10089−10092.
(40) Sitkoff, D.; Sharp, K. A.; Honig, B. *J. Phys. Chem.* **1994**, *98*, 1978−1988.
(41) Weise, J.; Shenkin, P. S.; Still, W. C. *J. Comput. Chem.* **1999**, *20*, 217−230.
(42) Baker, N. A.; Sept, D.; Joseph, S.; Holst, M. J.; McCammon, J. A. *Proc. Natl. Acad. Sci. U.S.A.* **2001**, *98*, 10037−10041.
(43) Hou, T.; Wang, J.; Li, Y.; Wang, W. *J. Chem. Inf. Model.* **2011**, *51*, 69−82.
(44) Wang, W.; Kollman, P. A. *Proc. Natl. Acad. Sci. U.S.A.* **2001**, *98*, 14937−14942.
(45) Hou, T.; Yu, R. *J. Med. Chem.* **2007**, *50*, 1177−1188.
(46) Ode, H.; Matsuyama, S.; Hata, M.; Hoshino, T.; Kakizawa, J.; Sugiura, W. *J. Med. Chem.* **2007**, *50*, 1768−17777.
(47) Wittayanarakul, K.; Aruksakunwong, O.; Saen-oon, S.; Chantratita, W.; Parasuk, V.; Sompornpisut, P.; Hannongbua, S. *Biophys. J.* **2005**, *88*, 867−879.
(48) Stoica, I.; Sadiq, S. K.; Coveney, P.V. *J. Am. Chem. Soc.* **2008**, *130*, 2639−2648.
(49) Naïm, M.; Bhat, S.; Rankin, K. N.; Dennis, S.; Chowdhury, S. F.; Siddiqi, I.; Drabik, P.; Sulea, T.; Bayly, C. I.; Jakalian, A.; et al. *J. Chem. Inf. Model.* **2007**, *47*, 122−133.
(50) Chen, W.; Chang, C. E.; Gilson, M. K. *Biophys. J.* **2004**, *87*, 3035−3049.
(51) Gohlke, H.; Kiel, C.; Case, D. A. *J. Mol. Biol.* **2003**, *330*, 891−913.
(52) Li, H.; Robertson, A. D.; Jensen, J. H. *Proteins* **2005**, *61*, 704−72.
(53) Adachi, M.; Ohhara, T.; Kurihara, K.; Tamada, T.; Honjo, E.; Okazaki, N.; Arai, S.; Shoyama, Y.; Kimura, K.; Maatsumura, H.; et al. *Proc. Natl. Acad. Sci. U.S.A.* **2009**, *106*, 4641−4646.
(54) Chen, J.; Yang, M.; Hu, G.; Shi, S.; Yi, C.; Zhang, Q. *J. Mol. Model.* **2009**, *15*, 1245−1252.
(55) Zoete, V.; Michielin, O.; Karplus, M. *J. Mol. Biol.* **2002**, *315*, 21−52.
(56) Tzoupis, H.; Leonis, G.; Durdagi, S.; Mouchlis, V.; Mavromoustakos, T.; Papadopoulos, M. G. *J. Comput.-Aided Mol. Des.* **2011**, *25*, 959−976.
(57) Zhu, Z. W.; Schuster, D. I.; Tuckerman, M. E. *Biochemistry* **2003**, *42*, 1326−1333.
(58) Piana, S.; Carloni, P.; Rothlisberger, U. *Protein Sci.* **2002**, *11*, 2393−2402.
(59) Perryman, A. L.; Lin, J. H.; McCammon, J. A. *Protein Sci.* **2004**, *13*, 1108−1123.
(60) Chong, L. T.; Duan, Y.; Wang, L.; Massova, I.; Kollman, P. A. *Proc. Natl. Acad. Sci. U.S.A.* **1999**, *96*, 14330−14335.
(61) Knecht, V. *J. Phys. Chem. B* **2010**, *114*, 12701−12707.
(62) Chang, C. A.; Chen, W.; Gilson, M. K. *Proc. Natl. Acad. Sci. U.S.A.* **2007**, *104*, 1534−1539.
(63) Höfinger, S.; Zerbetto, F. *Chem. Phys. Lett.* **2009**, *480*, 313−317.
(64) Liu, F.; Kovalevsky, A. Y.; Tie, Y.; Ghosh, A. K.; Harrison, R. W.; Weber, I. T. *J. Mol. Biol.* **2008**, *381*, 102−115.
(65) Shen, C.-H.; Wang, Y.-F.; Kovalevsky, A. Y.; Harrison, R. W.; Weber, I. T. *FEBS J.* **2010**, *277*, 3699−3714.